Supporting Information for "Using satellite observations to evaluate model microphysical representation of Arctic mixed-phase clouds"

J. K. Shaw[1] *, Z. S. McGraw[1] †, O. Bruno[2], T. Storelvmo[1,3], and S. Hofer[1]

[1]Department of Geosciences, University of Oslo, Oslo, Norway

[2]Karlsruhe Institute of Technology, Institute of Meteorology and Climate Research

[3]School of Business, Nord University, Bodø, Norway

Contents of this file

1. Text S1 - S5
2. Table S1

J. Shaw (jonah.shaw@colorado.edu)

*Now at Department of Atmospheric and Oceanic Sciences, University of Colorado, Boulder, Colorado, USA

†Now at Department of Applied Physics and Applied Mathematics, Columbia University and NASA Goddard Institute for Space Studies

3. Figures S1 - S5

Text S1. Validation of cloud-bulk SLF metric. We use new cloud products (Guzman et al., 2017) to study the CALIOP's ability to sample Arctic clouds (Fig. S1). On the annual mean, opaque clouds make up 56% of cloudy scenes and are sampled through an average depth of 1.17km. While more opaque clouds are present in the summer and fall, the sampling depth never falls below 1km, indicating that the cloud-bulk metric samples a distinct thermodynamic regime below the supercooled liquid layer for all seasons.

Text S2. Calculation of observated and modelled SLF metrics. Observed SLF is calculated as the ratio of the number of liquid cloud top pixels to the sum of ice plus liquid cloud top pixels following the methods of Bruno, Hoose, Storelvmo, Coopman, and Stengel (2021). Modelled SLF is calculated as the ratio of cloud liquid surface area density to the sum of liquid and ice surface area densities using the methods of Tan, Storelvmo, and Zelinka (2016). Observations are binned into $1^\circ \times 1^\circ$ gridcells for comparison with model output. Improved comparability of observed and modelled SLF metrics would require the creation of additional GOCCP and COSP2 output fields.

Text S3. Description of limit on secondary ice nucleation. The ice number tendency variable from secondary nucleation processes ("nsacwi") is limited to $10^6 \mathrm{kg}^{-1}$ per microphysics timestep (5 minutes) if it exceeds this value after the Hallet-Mossop secondary ice scheme runs. We only set a cap on the number production, which otherwise would have no limit, unlike the mass term that is subject to cloud mass conservation. We choose a very high cap in order to prevent errors from re-implementing the Hallet-Mossop parameterization that was effectively removed from the model due to the ice number error. Sensitivity tests without the secondary ice limit showed negligible changes in SLF,

confirming the dominant contribution of ice from heterogeneous processes when the model error is removed.

Text S4. Tuning Methods. The rate of ice and snow growth via the WBF process is highly-dependent on in-cloud conditions (updraft speed, concentration of cloud droplets and ice crystals) (Korolev, 2007). Previous studies reduced the efficiency of the WBF process in CAM5 by factors up to 10 to increase cloud liquid (Tan et al., 2016; Huang et al., 2021). We perform an identical modification in CAM6 to modify the WBF rate.

Tan et al. (2016) also modified the fraction of dust aerosols active as ice nuclei, presenting results with multipliers of 0.79 and 0.19. We perform a similar modification by scaling the aerosol concentration variables that are fed into the Hoose heterogeneous ice nucleation scheme ("total_aer_num", "coated_aer_num", "uncoated_aer_num", "total_interstitial_aer_num" ,"total_cloudborne_aer_num") (Hoose et al., 2008). We initially tested WBF rate multipliers between 0.1 and 10, and INP multipliers between 0.01 and 100. WBF multipliers significantly greater than 1 have not been previously used, and we found that values greater than 2 significantly reduced SLF in both metrics. INP multipliers varying over several orders of magnitude are reasonable, since observations exhibit high variability (DeMott et al., 2010) and our model variants respond differently to changes in these parameters.

Text S5. Evaluation of Ice Crystal Concentrations. We wish to evaluate whether our simulations have ice crystal concentrations that are reasonably consistent with observations. Observations of INP concentrations from the M-PACE field experiment (Prenni et al., 2009) provide one of the few records of INP concentrations for low- and mid-level Arctic clouds. We note that while there is not necessarily a 1-to-1 relationship between

INP concentrations and ice crystal number concentration, INP concentrations are a useful indication of what ice crystal number concentrations are reasonable. Prenni et al. (2009) report a mean INP concentration of $0.7\mathrm{L}^{-1}$ and a maximum INP concentration of $60\mathrm{L}^{-1}$. Prenni et al. (2009) note that INPs greater than 1.5µm were not measured, excluding some INPs from analysis. Ice crystal concentration in our fitted model simulations fall near the values reported by Prenni et al. (2009), indicating that ice crystals are reasonably reproduced by the models. The authors note that a strict comparison between our model output and observations from M-PACE would require specific knowledge of the cloud conditions during the field experiment and targeted modelling experiments beyond the scope of this study.

References

Bruno, O., Hoose, C., Storelvmo, T., Coopman, Q., & Stengel, M. (2021). Exploring the cloud top phase partitioning in different cloud types using active and passive satellite sensors. *Geophysical Research Letters*, *48*(2), e2020GL089863. Retrieved from https://agupubs.onlinelibrary.wiley.com/doi/abs/10.1029/2020GL089863 (e2020GL089863 2020GL089863) doi: https://doi.org/10.1029/2020GL089863

DeMott, P. J., Prenni, A. J., Liu, X., Kreidenweis, S. M., Petters, M. D., Twohy, C. H., ... Rogers, D. C. (2010). Predicting global atmospheric ice nuclei distributions and their impacts on climate. *Proceedings of the National Academy of Sciences*, *107*(25), 11217–11222. Retrieved from https://www.pnas.org/content/107/25/11217 doi: 10.1073/pnas.0910818107

Guzman, R., Chepfer, H., Noel, V., Vaillant de Guélis, T., Kay, J. E., Raberanto,

P., ... Winker, D. M. (2017). Direct atmosphere opacity observations from calipso provide new constraints on cloud-radiation interactions. *Journal of Geophysical Research: Atmospheres*, *122*(2), 1066-1085. Retrieved from https://agupubs.onlinelibrary.wiley.com/doi/abs/10.1002/2016JD025946 doi: https://doi.org/10.1002/2016JD025946

Hoose, C., Lohmann, U., Bennartz, R., Croft, B., & Lesins, G. (2008). Global simulations of aerosol processing in clouds. *Atmospheric Chemistry and Physics*, *8*(23), 6939–6963. Retrieved from https://www.atmos-chem-phys.net/8/6939/2008/ doi: 10.5194/acp-8-6939-2008

Huang, Y., Dong, X., Kay, J. E., Xi, B., & McIlhattan, E. A. (2021, May 01). The climate response to increased cloud liquid water over the arctic in cesm1: a sensitivity study of wegener–bergeron–findeisen process. *Climate Dynamics*, *56*(9), 3373-3394. Retrieved from https://doi.org/10.1007/s00382-021-05648-5 doi: 10.1007/s00382-021-05648-5

Korolev, A. (2007). Limitations of the wegener–bergeron–findeisen mechanism in the evolution of mixed-phase clouds. *Journal of the Atmospheric Sciences*, *64*(9), 3372-3375. Retrieved from https://doi.org/10.1175/JAS4035.1 doi: 10.1175/JAS4035.1

Prenni, A. J., Demott, P. J., Rogers, D. C., Kreidenweis, S. M., Mcfarquhar, G. M., Zhang, G., & Poellot, M. R. (2009). Ice nuclei characteristics from m-pace and their relation to ice formation in clouds. *Tellus B: Chemical and Physical Meteorology*, *61*(2), 436-448. Retrieved from https://www.tandfonline.com/doi/abs/10.1111/j.1600-0889.2008.00415.x doi: 10.1111/j.1600-0889.2008.00415.x

Tan, I., Storelvmo, T., & Zelinka, M. D. (2016). Observational constraints on mixed-phase clouds imply higher climate sensitivity. *Science*, *352*(6282), 224–227. Retrieved from https://science.sciencemag.org/content/352/6282/224 doi: 10.1126/science.aad5300

Run name	Total Cloud Bias (%)	Liquid Cloud Bias (%)	Ice Cloud Bias (%)	Undefined Cloud Bias (%)	Shortwave CRE Bias (W/m^2)	Longwave CRE Bias (W/m^2)
CAM6-Oslo	-2.0	-0.7	0.7	-1.8	-3.5	-0.1
CAM6	2.1	11.2	-7.9	-0.8	-4.0	-0.8
CAM6-OsloIce	-5.8	-8.2	6.1	-3.4	-2.9	0.3
CAM6-Oslo Fit 1	-3.6	-2.2	1.1	-2.2	-3.0	-0.6
CAM6-OsloIce Fit 2	-2.0	-0.9	1.6	-2.4	-3.7	0.4
CAM6-OsloIce Fit 3	-0.3	-1.3	3.6	-2.3	-5.1	1.8
CAM6 Fit 4	-5.1	5.4	-8.1	-2.0	-3.3	-1.9
CAM6-Olso(1.25,1)	-2.8	-1.5	1.0	-2.0	-3.1	-0.4
CAM6-Olso(1,10)	-2.8	-1.4	0.8	-1.9	-3.4	-0.3
CAM6-OsloIce(0.2,1)	-2.1	-6.4	7.6	-3.0	-5.5	2.5
CAM6-OsloIce(0.5,1)	-4.2	-6.8	6.1	-3.1	-4.1	1.2
CAM6-OsloIce(1,0.05)	-4.3	-3.3	2.1	-2.8	-2.2	-0.7
CAM6-OsloIce(1,0.1)	-4.9	-4.3	2.6	-2.9	-2.2	-0.8

Table S1. Annual model cloud biases for the region 66°N-82°N. Cloud cover biases are calculated relative to CALIOP GOCCP observations. Surface cloud radiative effect (CRE) biases are calculated relative to CERES-EBAF observations using a positive downward sign convention.

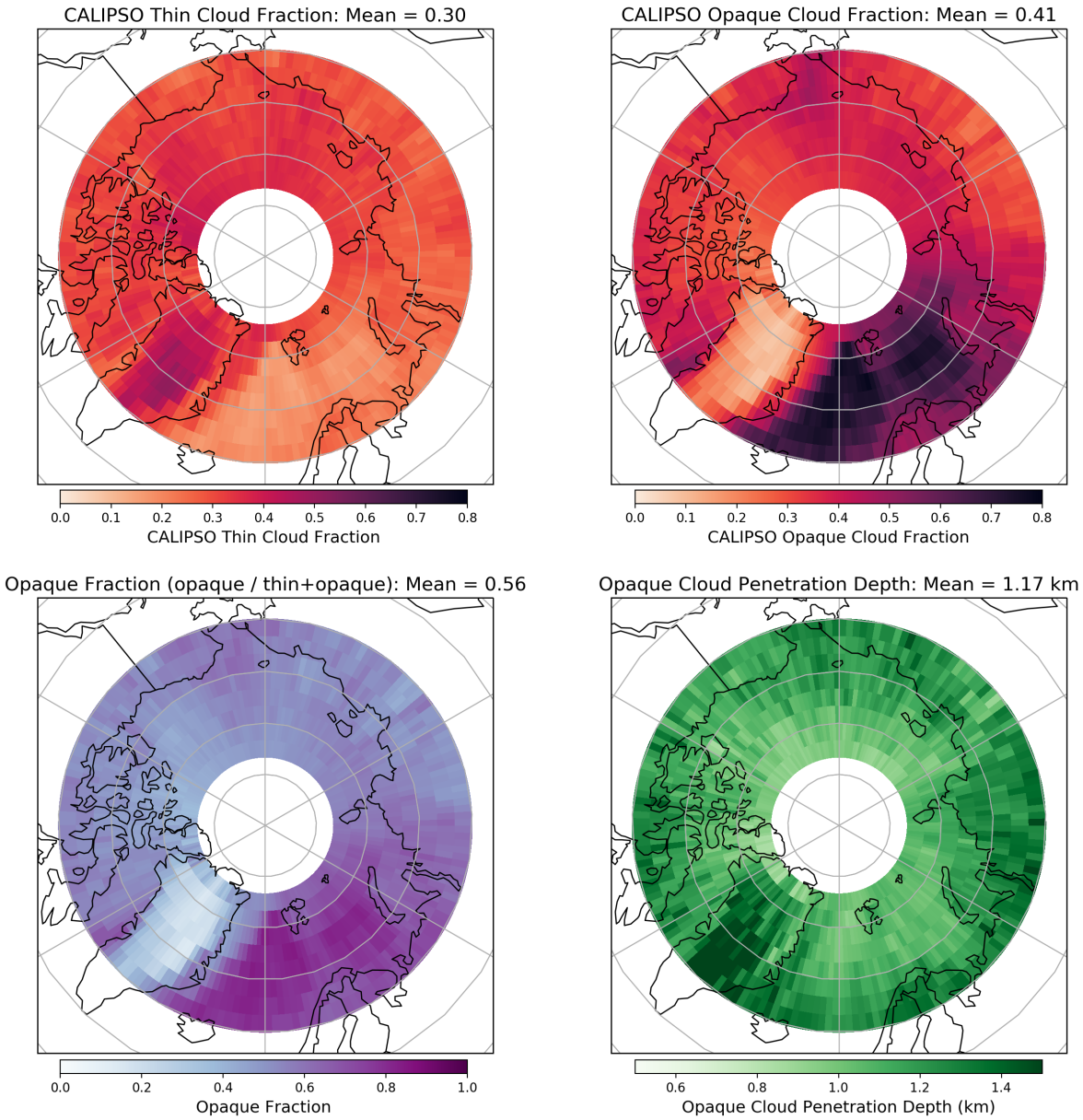

Figure S1. Arctic maps (66–90°N) of a) Thin Cloud Fraction from CALIOP, b) Opaque Cloud Fraction from CALIOP, c) Opaque Fraction (opaque cloud fraction / total cloud fraction) from CALIOP, and d) Cloud sampling depth from CALIOP. Cloud sampling depth is computed as the difference between cloud height and opacity height using cloud opacity products developed in Guzman et al. (2017). Mean values are computed as the area-weighted average of the plotted region.

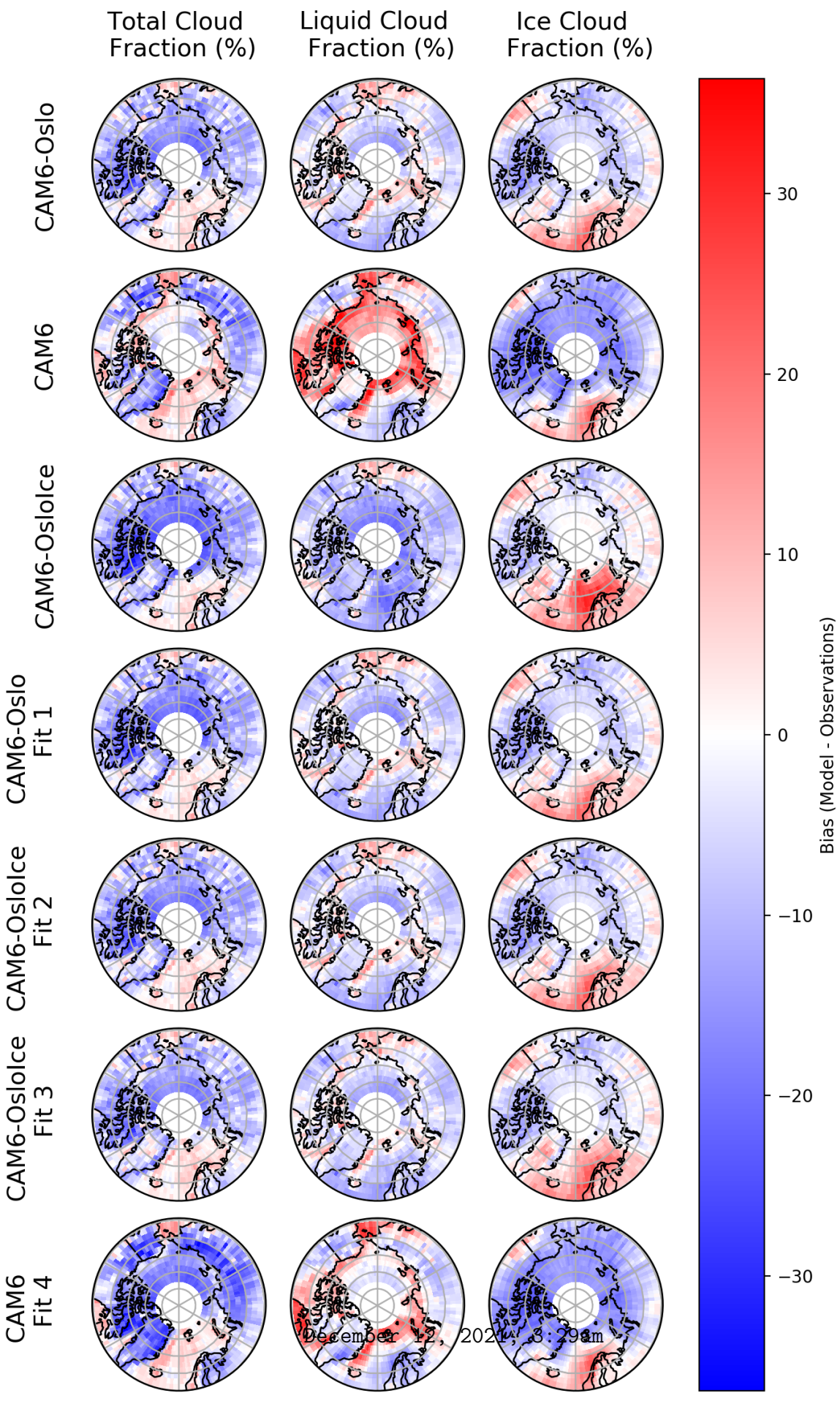

Figure S2. North Pole maps (60–82°N) of cloud cover bias by CALIOP phase designation.

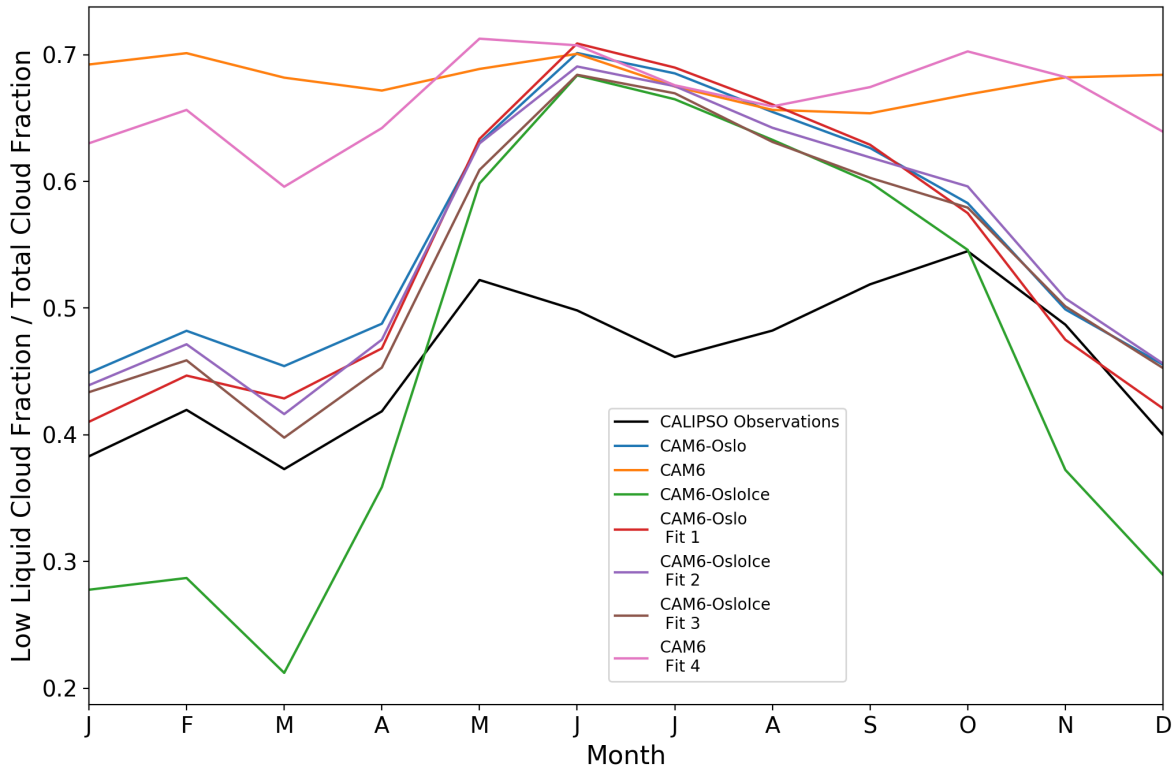

Figure S3. Monthly values for the fraction of total cloud made up of low-level liquid phase clouds (low-level liquid cloud fraction / total cloud fraction). Observations are taken from the CALIOP GOCCP cloud product. Model values are computed using variables from the COSP satellite simulator package.

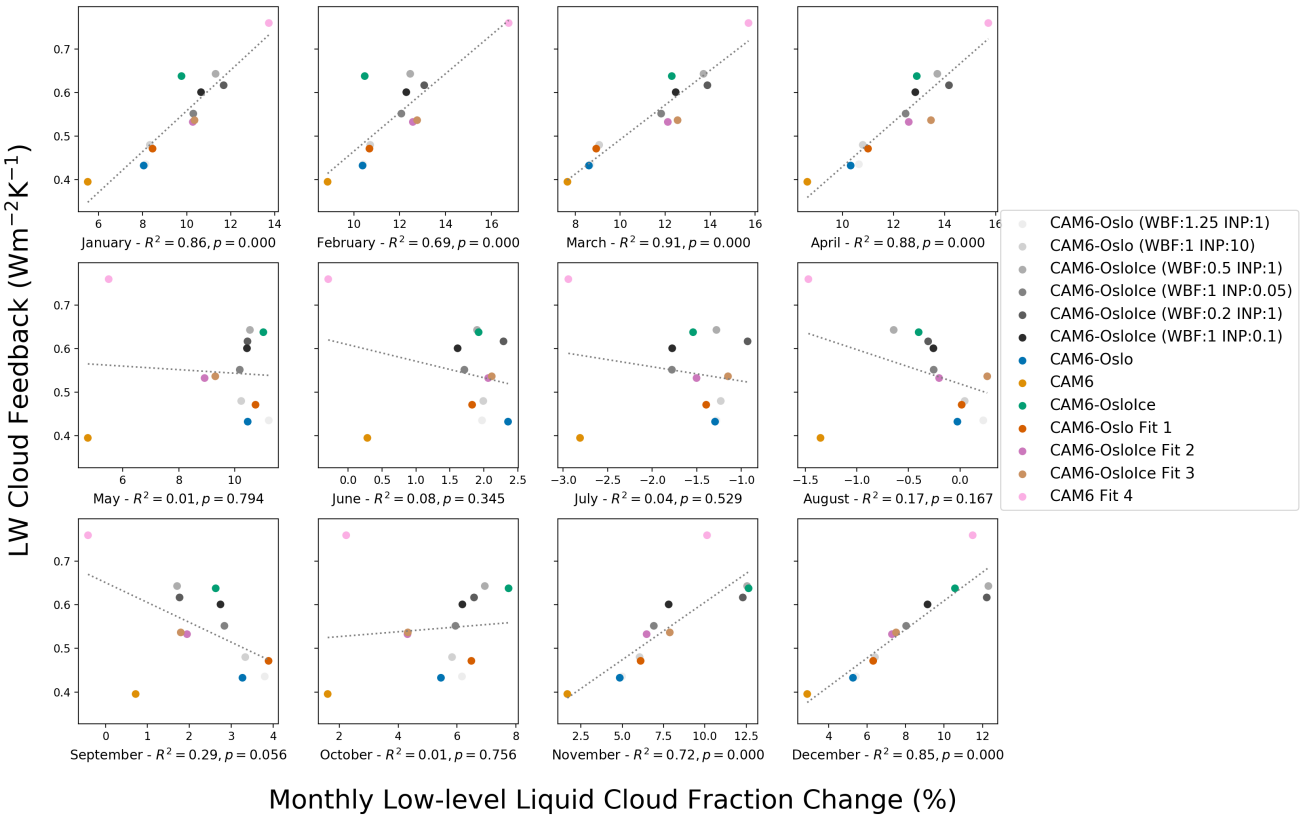

Figure S4. Longwave cloud feedback as a function of the change in low-level liquid cloud fraction between present day and +4K simulations by month.

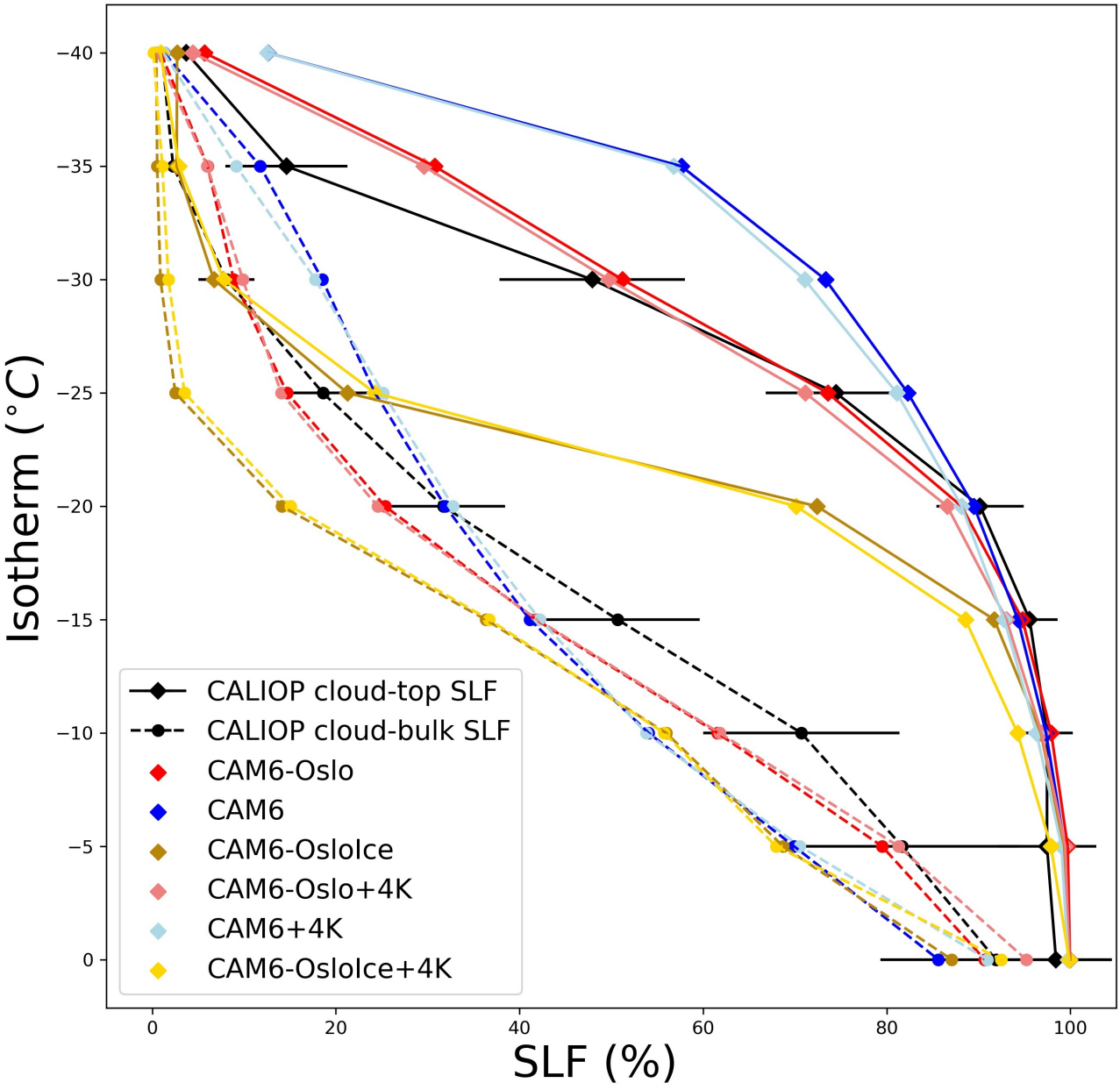

Figure S5. Supercooled liquid fraction by isotherm for cloud-top and cloud-bulk metrics for present-day base model simulations and +4K base model simulations. Error bars on CALIOP SLF values correspond to one standard deviation. All values represent **an area-weighted** average from 66°-82°N.